Astron. Astrophys. 355, 835–847 (2000)

ASTRONOMY AND ASTROPHYSICS

Investigations of the Local Supercluster velocity field

III. Tracing the backside infall with distance moduli from the direct Tully-Fisher relation

T. Ekholm[1,2], **P. Lanoix**[1], **P. Teerikorpi**[2], **P. Fouqué**[3], **and G. Paturel**[1]

[1] CRAL - Observatoire de Lyon, 69561 Saint Genis Laval CEDEX, France
[2] Tuorla Observatory, 21500 Piikkiö, Finland
[3] ESO, Santiago, Chile

Received 20 December 1999 / Accepted 25 January 2000

Abstract. We have extended the discussion of Paper II (Ekholm et al. 1999a) to cover also the backside of the Local Supercluster (LSC) by using 96 galaxies within $\Theta < 30^\circ$ from the adopted centre of LSC and with distance moduli from the direct B-band Tully-Fisher relation. In order to minimize the influence of the Malmquist bias we required $\log V_{\rm max} > 2.1$ and $\sigma_{B_T} < 0.2^{\rm mag}$.

We found out that if $R_{\rm Virgo} < 20$ Mpc this sample fails to follow the expected dynamical pattern from the Tolman-Bondi (TB) model. When we compared our results with the Virgo core galaxies given by Federspiel et al. (1998) we were able to constrain the distance to Virgo: $R_{\rm Virgo} = 20 - 24$ Mpc.

When analyzing the TB-behaviour of the sample as seen from the origin of the metric as well as that with distances from the extragalactic Cepheid PL-relation we found additional support to the estimate $R_{\rm Virgo} = 21$ Mpc given in Paper II. Using a two-component mass-model we found a Virgo mass estimate $M_{\rm Virgo} = (1.5 - 2) \times M_{\rm virial}$, where $M_{\rm virial} = 9.375 \times 10^{14} M_\odot$ for $R_{\rm Virgo} = 21$ Mpc. This estimate agrees with the conclusion in Paper I (Teerikorpi et al. 1992).

Our results indicate that the density distribution of luminous matter is shallower than that of the total gravitating matter when $q_0 \leq 0.5$. The preferred exponent in the density power law, $\alpha \approx 2.5$, agrees with recent theoretical work on the universal density profile of dark matter clustering in an Einstein-deSitter universe (Tittley & Couchman 1999).

Key words: cosmology: theory – cosmology: dark matter – cosmology: distance scale – galaxies: distances and redshifts – galaxies: general – galaxies: kinematics and dynamics

1. Introduction

Study of the local extragalactic velocity field has a considerable history. Rubin (1988) pinpoints the beginning of the studies concerning deviations from the Hubble law to a paper of Gamow (1946) where Gamow asked if galaxies partake of a large-scale systematic rotation in addition to the Hubble expansion. The pioneer works by Rubin (1951) and Ogorodnikov (1952) gave evidence that the local extragalactic velocity field is neither linear nor isotropic. De Vaucouleurs (1953) then interpreted the distribution of bright galaxies and proposed rotation in terms of a flattened local supergalaxy. This short but remarkable paper did not yet refer to differential expansion, introduced by de Vaucouleurs (1958) as an explanation of the "north-south anisotropy" which he stated was first pointed out by Sandage (Humason et al. 1956). Differential expansion was a milder form of Hubble's "the law of redshifts does not operate within the Local Group" and de Vaucouleurs pondered that "in condensed regions of space, such as groups or clusters, the expansion rate is greatly reduced...". Though there was a period of debate on the importance of the kinematic effects claimed by de Vaucouleurs and even on the reality of the local supergalaxy (presently termed as the Local Supercluster, LSC), already for two decades the reality of the differential peculiar velocity field around the Virgo cluster has been generally accepted. However, its amplitude and such details as the deviation from spherical symmetry and possible rotational component, are still under discussion.

A theoretical line of research related to de Vaucouleurs' differential expansion, has been motivated by the work on density perturbations in Friedmann cosmological models, resulting in infall models of matter (Silk 1974) which predict a connection between the infall peculiar velocity at the position of the Local Group towards the Virgo cluster and the density parameter of the Friedmann universe. Later on, Olson & Silk (1979) further developed the formalism in a way which was found useful in Teerikorpi et al. (1992; hereafter Paper I). The linearized approximation of Peebles (1976) has been often used for describing the velocity field and for making routine corrections for systemic velocities.

Using Tolman-Bondi model (Tolman 1934, Bondi 1947) Hoffman et al. (1980) calculated the expected velocity dispersions along line-of-sight as a function of angular distance from a supercluster and applied the results to Virgo. They derived a

Send offprint requests to: T. Ekholm

gravitating mass of about $4\times10^{14}M_\odot\times100/h_0$ inside the cone of 6°. The Tolman-Bondi (TB) model is the simplest inhomogeneous solution to the Einstein's field equations. It describes the time evolution of a spherically symmetric pressure-free dust universe in terms of comoving coordinates. For details of the TB-model cf. Ekholm et al. (1999a; hereafter Paper II).

Then, following the course of Hoffman et al. (1980), Tully & Shaya (1984) calculated the expected run of radial velocity vs. distance at different angular distances from Virgo and for different (point) mass-age models. Comparison of such envelope curves with available galaxy data agreed with the point mass having roughly the value of Virgo's virial mass ($7.5\times10^{14}M_\odot\times75/h_0$) for reasonable Friedmann universe ages.

The Hubble diagram of Tully & Shaya contained a small number of galaxies and did not very well show the expected behaviour. With a larger sample of Tully-Fisher measured galaxies and attempting to take into account the Malmquist bias, Teerikorpi et al. (1992) were able to put in evidence the expected features: an initial steeply rising tight velocity-distance relation, the local maximum in front of Virgo and the final ascending part of the relation, expected to approach asymptotically the undisturbed Hubble law. Looking from the Virgo centre the zero-velocity surface was clearly seen around $r/R_{\rm Virgo}\approx0.5$. Using either a continuous mass model or a two-component model, the conclusions of Tully & Shaya (1984) were generally confirmed and it was stated that "Various density distributions, constrained by the mass inside the Local Group distance (required to produce $V_{\rm Virgo}$), agree with the observations, but only if the mass within the Virgo 6° region is close to or larger than the standard Virgo virial mass values. This is so independently of the value of q_0, of the slope of the density distribution outside of Virgo, and of the values adopted for Virgo distance and velocity".

It is the aim of the present paper to use the available sample of galaxies with more accurate distances from Cepheids and Tully-Fisher relation to study the virgocentric velocity field. In Paper II galaxies with Cepheid-distances were used to map the velocity field in front of Virgo, here we add galaxies with good Tully-Fisher distances in order to see both the frontside and backside behaviour and investigate how conclusions of Paper I should be modified in the light of new data. It should be emphasized that also our Tully-Fisher distances are now better, after a programme to study the slope and the Hubble type dependence of the zero-point (see Theureau et al. 1997).

This paper is structured as follows. In Sect. 2 we shortly review the basics of the use of the direct Tully-Fisher relation, give the relation to be used and describe our sample and the restrictions put upon it. In Sect. 3 we examine our sample in terms of systemic velocity vs. distance diagrams and see which distance to Virgo will bring about best agreement between the TB-predictions and the observations. In Sect. 4 we try to answer the question whether we have actually found the Virgo cluster at the centre of the TB-metric. In Sect. 5 we re-examine our sample from a virgocentric viewpoint and compare our results from the TF-distances with the sample of galaxies with distances from the extragalactic Cepheid PL-relation. In Sect. 6 we shortly discuss the mass estimate and our density profile and, finally, in Sect. 7 we summarize our results with some conclusive remarks.

2. The sample based on direct B-band Tully-Fisher relation

The absolute magnitude M and the logarithm of the maximum rotational velocity $\log V_{\rm max}$ of a galaxy (for which also a shorthand p is used) are related as:

$$M=a\log V_{\rm max}+b. \tag{1}$$

The use of this kind of relation as a distance indicator was suggested by Gouguenheim (1969). Eq. 1 is known as Tully-Fisher (TF) relation after Tully & Fisher (1977).

It is nowadays widely acknowledged that the distance moduli inferred using Eq. 1 are underestimated because of selection effects in the sampling. We can see how this Malmquist bias affects the distance determination by considering the *observed* average absolute magnitude $\langle M\rangle_p$ at each p as a function of the true distance r. The limit in apparent magnitude, $m_{\rm lim}$, cuts off progressively more and more of the distribution function of M for a constant p. This means that the *observed* mean absolute magnitude $\langle M\rangle_p$ is overestimated by the expectation value $E(M|\,p)=ap+b$:

$$\langle M\rangle_p\le E(M|\,p), \tag{2}$$

This inequality gives a practical measure of the Malmquist bias depending primarily on p, r, σ_M and $m_{\rm lim}$. The equality holds only when the magnitude limit cuts the luminosity function $\Phi(M)$ insignificantly. For our present purposes it is also important to note that for luminous galaxies, which are also fast rotators (large p) the effect of the magnitude limit is felt at much larger distances than for intrinsically faint galaxies which rotate slowly. Hence by limiting p to large values one expects to add to the sample galaxies which suffer very little from the Malmquist bias within a restricted distance range. For this kind of bias the review by Teerikorpi (1997) suggested the name Malmquist bias of the $2^{\rm nd}$ kind, in order to make a difference from the classical Malmquist bias (of the $1^{\rm st}$ kind).

Following Paper I we selected galaxies towards Virgo by requiring $\log V_{\rm max}$ to be larger than 2.1. At the time Paper I was written this value was expected to bring about nearly unbiased TF distance moduli up to twice the Virgo distance. With the present, much deeper sample the limit chosen is much safer. Also, we allow an error in B-magnitude to be at maximum $0.2^{\rm mag}$. We also require the axis ratio to be $\log R_{25}>0.07$. Because the maximum amplitude of systemic velocities near Virgo can be quite large, we first restricted the velocities by $V_{\rm obs}<3V_{\rm Virgo}^{\rm cosm}\cos\Theta$, where Θ is the angular distance from the adopted centre ($l=284^\circ$, $b=74.5^\circ$) and the cosmological velocity of the centre is following Paper II $V_{\rm Virgo}^{\rm cosm}=1200\ {\rm km\,s^{-1}}$. After this the derived TF-distances were restricted by $R_{\rm TF}<60\ {\rm Mpc}$.

With these criteria we found 96 galaxies within $\Theta<30^\circ$ tabulated in Table 1, where in Columns (1) and (2) we give the PGC number and name (the superscript after some galaxies will be explained in Sect. 4). In Columns (3) and (4) the

Table 1. Basic information for the 96 galaxies accepted to our TF-sample within 30° from the centre. For an explanation of the entries cf. Sect. 2.

PGC	Name	l	b	T	$\log R_{25}$	$B_{\rm T}^{\rm c}$	σ_B	$\log V_{\rm max}$	$\sigma_{\log V_{\rm max}}$	$V_{\rm obs}$	$\Theta_{\rm gal}$	$R_{\rm gal}$
(1)	(2)	(3)	(4)	(5)	(6)	(7)	(8)	(9)	(10)	(11)	(12)	(13)
031883	NGC 3338	230.33	57.02	5.3	.21	11.02	.12	2.268	.033	1174	26.55	28.32
032007	NGC 3351	233.95	56.37	2.5	.23	9.97	.13	2.166	.027	640	26.18	11.52
032192	NGC 3368	234.44	57.01	1.5	.17	9.65	.12	2.318	.039	761	25.49	12.56
032306	NGC 3389	233.72	57.74	6.1	.35	11.52	.10	2.116	.029	1168	25.04	24.55
033166	NGC 3486	202.08	65.49	5.1	.14	10.55	.08	2.125	.050	632	26.83	15.54
033234	NGC 3495	249.89	54.73	5.9	.64	11.08	.08	2.233	.006	960	23.86	27.44
034612	NGC 3623	241.33	64.22	1.6	.61	9.36	.16	2.395	.005	676	17.60	13.51
034695	NGC 3627	241.97	64.42	2.7	.33	8.92	.16	2.265	.020	596	17.28	9.26
034697	NGC 3628	240.86	64.78	3.3	.59	9.19	.16	2.349	.009	719	17.28	13.14
034935	NGC 3655	235.59	66.97	4.9	.18	11.75	.08	2.260	.049	1364	17.02	38.80
035043	NGC 3666	246.40	64.18	5.2	.55	11.53	.07	2.108	.009	923	16.33	23.32
035088	NGC 3672	270.42	47.55	4.7	.31	11.28	.16	2.328	.018	1635	27.58	37.50
035224	NGC 3684	235.98	68.07	4.7	.18	11.51	.10	2.120	.032	1053	16.12	23.86
035268	NGC 3686	235.71	68.28	4.5	.10	11.51	.11	2.126	.055	1047	16.05	24.25
035294	NGC 3689	212.72	71.32	5.8	.19	12.43	.09	2.209	.040	2674	19.89	47.91
035405	NGC 3701	217.69	71.30	3.8	.32	12.73	.08	2.120	.021	2732	18.70	41.22
035440	NGC 3705	252.02	63.79	2.3	.38	11.10	.13	2.232	.022	871	15.28	19.44
036243	NGC 3810	252.94	67.22	5.6	.17	10.79	.09	2.246	.029	858	12.28	24.86
036266	NGC 3813	176.19	72.42	4.4	.29	11.52	.07	2.202	.029	1459	26.63	29.42
038031	NGC 4045	275.98	62.27	1.7	.20	12.27	.11	2.249	.051	1806	12.55	34.88
038150	NGC 4062	185.26	78.65	5.6	.35	11.04	.07	2.189	.011	743	20.48	23.94
038693	NGC 4145	154.27	74.62	6.6	.17	11.21	.08	2.106	.034	1032	27.89	15.65
038749	NGC 4152	260.39	75.42	4.9	.10	12.24	.16	2.194	.099	2059	6.15	40.73
038916	IC 769	269.75	72.44	3.8	.17	12.82	.11	2.180	.046	2093	4.53	50.47
038943	NGC 4178[1]	271.86	71.37	6.6	.46	10.86	.09	2.101	.037	245	4.73	13.14
038964	NGC 4180	276.79	67.94	3.2	.45	12.45	.18	2.301	.018	1935	6.95	51.85
039025	NGC 4189[2]	268.37	73.72	6.1	.17	11.97	.19	2.221	.086	1994	4.34	40.03
039028	NGC 4192[3]	265.44	74.96	2.4	.60	9.98	.09	2.377	.005	-253	4.89	17.13
039040	NGC 4193[4]	268.91	73.51	4.4	.32	12.43	.09	2.251	.018	2355	4.26	51.02
039152	IC 3061[5]	268.20	74.39	5.0	.74	12.90	.08	2.136	.017	2201	4.23	47.25
039224	NGC 4212[6]	268.89	74.36	5.6	.20	11.21	.15	2.175	.034	-198	4.05	24.93
039246	NGC 4216[7]	270.45	73.74	2.2	.65	9.96	.15	2.410	.005	11	3.78	18.54
039308	NGC 4222[8]	270.54	73.93	6.0	.79	12.30	.09	2.146	.007	111	3.70	38.11
039389	NGC 4235	279.18	68.47	1.0	.65	11.88	.09	2.153	.009	2263	6.22	22.53
039393	NGC 4237[9]	267.21	75.76	4.9	.19	11.92	.13	2.158	.034	757	4.47	31.92
039656	NGC 4260	281.56	67.63	1.0	.30	12.17	.06	2.388	.024	1695	6.91	48.36
039724	NGC 4274	191.40	82.62	1.4	.44	10.58	.17	2.357	.015	891	17.43	21.40
039738	NGC 4273	282.53	66.96	5.5	.21	11.74	.09	2.243	.031	2228	7.56	38.19
039886	NGC 4289	284.38	65.49	4.9	1.00	12.72	.09	2.232	.010	2381	9.01	56.26
039907	NGC 4293	262.85	78.82	1.3	.28	10.70	.13	2.229	.022	839	6.45	16.04
039974	NGC 4302[10]	272.52	75.68	5.3	.81	10.96	.14	2.236	.009	1005	3.17	25.28
040033	NGC 4307[11]	280.58	70.63	3.1	.66	11.65	.07	2.253	.012	956	4.00	31.54
040119	NGC 4316[12]	280.72	70.95	4.7	.70	12.27	.08	2.159	.012	1119	3.68	37.60
040153	NGC 4321[13]	271.14	76.90	4.6	.09	9.65	.11	2.277	.083	1483	3.97	15.44
040251	NGC 4343[14]	283.56	68.77	2.4	.53	12.26	.18	2.221	.009	867	5.73	32.21
040284	NGC 4348	289.61	58.71	4.2	.66	11.94	.15	2.244	.007	1815	15.93	39.95
040507	NGC 4380[15]	281.94	71.82	2.6	.24	12.03	.14	2.175	.045	839	2.75	30.48
040566	IC 3322A[16]	284.72	69.17	6.0	.89	11.87	.14	2.115	.012	852	5.33	28.77
040581	NGC 4388[17]	279.12	74.34	2.9	.55	10.76	.11	2.329	.006	2401	1.32	25.67
040621	UGC 7522	287.43	65.53	5.3	.95	12.75	.12	2.161	.013	1265	9.04	47.15
040644	NGC 4402[18]	278.79	74.78	4.4	.51	11.54	.19	2.152	.008	120	1.41	25.97
040692	NGC 4414	174.55	83.18	5.1	.23	10.28	.11	2.342	.033	694	18.87	24.56
040914	NGC 4438[19]	280.35	74.83	2.9	.47	10.08	.16	2.231	.018	-36	1.02	14.43
040988	NGC 4448	195.35	84.67	2.0	.43	11.22	.12	2.266	.009	618	16.25	22.51

Table 1. continued

PGC	Name	l	b	T	$\log R_{25}$	$B_{\rm T}^{\rm c}$	σ_B	$\log V_{\rm max}$	$\sigma_{\log V_{\rm max}}$	$V_{\rm obs}$	$\Theta_{\rm gal}$	$R_{\rm gal}$
(1)	(2)	(3)	(4)	(5)	(6)	(7)	(8)	(9)	(10)	(11)	(12)	(13)
041024	NGC 4450[20]	273.91	78.64	1.8	.12	10.48	.07	2.413	.047	1862	4.74	23.75
041317	NGC 4480	289.67	66.58	5.2	.31	12.36	.06	2.226	.017	2288	8.13	46.90
041517	NGC 4501[21]	282.33	76.51	4.1	.27	9.56	.12	2.476	.018	2172	2.05	24.87
041719	NGC 4519[22]	289.17	71.05	6.3	.09	11.96	.06	2.146	.189	1087	3.77	32.59
041789	NGC 4527	292.60	65.18	3.4	.41	10.47	.13	2.264	.014	1571	9.76	18.86
041812	NGC 4535[23]	290.07	70.64	4.8	.12	10.19	.16	2.311	.062	1821	4.26	21.69
041934	NGC 4548[24]	285.70	76.83	2.8	.08	10.58	.11	2.291	.078	379	2.37	21.34
042038	NGC 4565	230.77	86.44	3.6	.86	8.90	.19	2.414	.004	1181	13.66	15.54
042064	NGC 4567	289.78	73.75	5.2	.14	11.58	.09	2.243	.070	2145	1.75	34.28
042069	NGC 4568[25]	289.82	73.73	5.2	.34	10.82	.09	2.274	.010	2134	1.77	26.25
042089	NGC 4569[26]	288.47	75.62	2.7	.35	9.51	.17	2.369	.021	-355	1.61	16.07
042168	NGC 4579[27]	290.40	74.35	2.2	.08	10.12	.09	2.471	.047	1399	1.72	23.50
042319	NGC 4591	294.54	68.68	3.0	.30	13.26	.12	2.200	.027	2282	6.68	57.43
042476	NGC 4602	297.89	57.63	5.1	.47	10.99	.17	2.309	.008	2351	17.68	31.18
042741	NGC 4639[28]	294.30	75.98	3.3	.19	11.68	.07	2.254	.052	888	3.01	32.06
042791	NGC 4642	298.57	62.16	4.6	.53	12.32	.11	2.132	.050	2476	13.37	35.79
042816	NGC 4647[29]	295.75	74.34	5.4	.08	11.53	.14	2.127	.048	1298	3.15	24.54
042833	NGC 4651[30]	293.07	79.12	5.1	.18	10.81	.10	2.358	.031	711	5.05	32.73
042857	NGC 4654[31]	295.43	75.89	5.4	.22	10.46	.10	2.218	.037	926	3.23	19.14
043147	NGC 4682	301.23	52.79	4.4	.32	12.37	.10	2.191	.018	2126	22.81	42.25
043186	NGC 4689[32]	299.08	76.61	5.0	.08	11.20	.10	2.148	.073	1508	4.30	22.30
043254	NGC 4698	300.57	71.35	1.4	.16	11.00	.12	2.404	.054	872	5.77	29.45
043331	NGC 4701	301.54	66.25	4.6	.07	12.41	.08	2.106	.127	571	10.05	34.79
043451	NGC 4725	295.09	88.36	2.1	.18	9.57	.15	2.380	.042	1160	13.89	14.29
043601	NGC 4746[33]	303.39	74.95	3.9	.53	12.29	.06	2.208	.020	1667	5.10	42.62
043784	NGC 4771	304.03	64.14	4.9	.65	11.59	.13	2.109	.013	969	12.41	24.04
043798	NGC 4772	304.15	65.03	1.0	.23	11.52	.15	2.394	.041	884	11.63	36.43
043939	NGC 4793	101.55	88.05	5.4	.27	11.57	.12	2.248	.030	2466	17.45	34.58
044191	NGC 4818	305.21	54.32	2.8	.43	11.18	.10	2.136	.017	867	21.87	18.56
044254	UGC 8067	305.92	61.13	4.4	.73	12.75	.10	2.154	.017	2668	15.51	45.58
044392	NGC 4845	306.74	64.40	2.3	.61	11.12	.16	2.292	.007	1073	12.70	23.05
045170	NGC 4939	308.10	52.40	3.8	.36	11.07	.10	2.369	.020	2908	24.17	37.42
045311	NGC 4961	44.51	86.76	5.8	.17	13.41	.15	2.118	.043	2513	17.37	58.94
045643	NGC 4995	310.78	54.76	3.0	.16	11.42	.12	2.350	.041	1578	22.38	36.80
045749	NGC 5005	101.61	79.25	3.0	.30	9.92	.12	2.460	.009	967	26.24	24.77
045948	NGC 5033	98.06	79.45	5.1	.42	9.76	.16	2.341	.010	896	26.02	19.28
046441	NGC 5073	312.94	47.48	3.7	.75	12.08	.18	2.281	.014	2533	29.74	47.06
046671	NGC 5112	96.06	76.76	5.3	.13	12.12	.09	2.112	.067	1003	28.67	30.93
048130	NGC 5248	335.93	68.75	4.1	.11	10.44	.18	2.283	.083	1048	16.70	22.23
049555	NGC 5364	340.71	63.03	5.4	.18	10.56	.19	2.239	.043	1128	22.28	21.20
050782	NGC 5506	339.15	53.81	3.7	.57	11.65	.19	2.174	.015	1679	29.79	28.98
051233	NGC 5566	349.27	58.56	1.3	.46	10.66	.18	2.378	.040	1408	28.30	23.49

galactic coordinates l, b in degrees are given. In Column (5) we give the morphological type code T and in Column (6) we give the logarithm of the axis ratio at $25\ ^{\rm mag}/\Box''$, $\log R_{25}$. The total B-magnitude corrected according to RC3 (de Vaucouleurs et al. 1991)[1] and the corresponding weighted mean error are given in Columns (7) and (8). In Columns (9) and (10) we give the logarithm of the maximum rotational velocity $\log V_{\rm max}$ with the weighted mean error. In Column (11) we give the observed velocity $V_{\rm obs}$ by which – as in Paper II – we mean the mean observed heliocentric velocity corrected to the centroid of the Local Group according to Yahil et al. (1977). Finally, in Columns (12) and (13) we have the angular distance $\Theta_{\rm gal}$ in degrees between a galaxy and the centre and the distance $R_{\rm gal}$ in Mpc from us calculated using the direct TF-relation given below. The data in Columns (1) – (11) were extracted from the Lyon-Meudon extragalactic database LEDA.

Our direct TF-parameters for the B-band magnitudes were taken from Theureau et al. (1997). The slope for the relation is $a = -5.823$ and the zero-points corrected for the type-effect are

[1] Except for galactic extinction which is adopted from RC2 (de Vaucouleurs et al. 1976)

Table 2. Type-corrected zero-points.

Hubble type code T	zero-point b
1,2	-7.347
3	-7.725
4	-8.001
5	-8.034
6	-8.109
7,8	-7.499

given in Table 2. The calibration of the zero-points was based on a sample of galaxies with Cepheid distances given in Table 1 in Theureau et al. (1997). This calibration corresponded to a Hubble constant $H_0 \approx 55\,\mathrm{km\,s^{-1}\,Mpc^{-1}}$.

Finally we comment on our notation on velocities. We use systemic velocity in the same sense as in Paper II, i.e. the systemic velocity is a combination of the cosmological velocity and the velocity induced by Virgo with the assumption that the virgocentric motions dominate. When we refer to observed systemic velocity we call it $V_{\rm obs}$ and when to model prediction, $V_{\rm pred}$. If we make no distinction, we use $V_{\rm sys}$.

3. The $V_{\rm sys}$ vs. $R_{\rm gal}$ diagram for the TF-sample

In Paper II we found a TB-solution using a simple density law $\rho(R) = \rho_{\rm bg}(1 + kR^{-\alpha})$, which fitted data quite well. Here R is the distance from the origin of the TB-metric, α is the density gradient and k the density contrast. Because an Einstein-deSitter universe was assumed, the background density $\rho_{\rm bg}$ equals the critical cosmological density, $\rho_{\rm c}$. The relevant quantity, the mass within a radius d, the radius R in units of Virgo distance, was expressed as $M(d) = M(d)_{\rm EdS} \times (1 + k'd^{-\alpha})$ (cf. Eq. 9 in Paper II). Here k' is the mass excess within a sphere having a radius of one Virgo distance.

Unfortunately, the sample of galaxies with distances from the extragalactic Cepheid PL-relation did not reach well enough behind the LSC. Our present sample is clearly deep enough to reveal the backside infall signal. In Paper I it was well seen how in the front the differences between different TB-models were not large, in contrast to the background, where the model predictions progressively deviate from each other.

In the formalism developed by Ekholm (1996) and adopted in Paper II, the quantity given by Eq. 8 in Paper II, $A(d, q_0)$, which is needed for solving the development angle, is no longer an explicit function of H_0. There are – however – still rather many free parameters, which we shortly discuss below:

1. The deceleration parameter q_0. In Paper II we considered q_0 given, restricting our analysis to the Einstein-deSitter universe ($q_0 = 0.5$). In Paper I it was concluded that q_0 has a minor influence on the $V_{\rm pred}$ vs. $R_{\rm gal}$ curves and on the Virgo mass (though it has a large effect on total mass inside the LG sphere).
2. The density gradient α and the relative mass excess at $d = 1$, k'. We remind that k' in our formalism does not depend on α but only on the amount by which the LG's expansion velocity with respect to centre of LSC has slowed down. In our two-component model (Sect. 5) k' will depend also on α.
3. The velocities $V_{\rm LG}^{\rm in}$, $V_{\rm Virgo}^{\rm obs}$ and $V_{\rm Virgo}^{\rm cosm}$. As in Papers I and II, we presume Virgo to be at rest with cosmological background: $V_{\rm Virgo}^{\rm cosm} = V_{\rm LG}^{\rm in} + V_{\rm Virgo}^{\rm obs}$. We feel that our choices for the infall velocity of the Local Group $V_{\rm LG}^{\rm in} = 220\,\mathrm{km\,s^{-1}}$ and for the observed velocity of Virgo $V_{\rm Virgo}^{\rm obs} = 980\,\mathrm{km\,s^{-1}}$ are relatively safe.

We would also like to remind that our solutions in Paper II had an implicit dependence on the Hubble constant H_0, because we fixed our distance to Virgo kinematically from $R_{\rm Virgo} = V_{\rm Virgo}^{\rm cosm}/H_0$ by adopting $H_0 = 57\,\mathrm{km\,s^{-1}\,Mpc^{-1}}$. This *global* value was based on SNe Ia (Lanoix 1999) and agrees also with the more local results of the KLUN (Kinematics of the Local Universe) project (Theureau et al. 1997; Ekholm et al. 1999b) and with the findings of Federspiel et al. (1998). Here we allow the distance of Virgo, or equivalently the Hubble constant H_0, vary keeping the cosmological velocity of Virgo fixed. This choice is justified because even though the estimates for H_0 have converged to $\sim 60\,\mathrm{km\,s^{-1}\,Mpc^{-1}}$ the reported 1σ errors are not small and the different values are still scattered (50-70 $\mathrm{km\,s^{-1}\,Mpc^{-1}}$).

In this section we examine how well the present TB-sample agrees with the Model 1 of Paper II, which constitutes of a density excess embedded in a FRW universe with $q_0 = 0.5$ and $H_0 = 57\,\mathrm{km\,s^{-1}\,Mpc^{-1}}$. The model parameters are $k' = 0.606$ and $\alpha = 2.85$, which predict for the Virgo cluster ($\Theta < 6^\circ$) a mass $1.62 \times M_{\rm virial}$, where $M_{\rm virial}$ is the virial mass of the Virgo cluster derived by Tully & Shaya (1984) $= 7.5 \times 10^{14} M_\odot R_{\rm Virgo}/16.8\,\mathrm{Mpc}$. Because of fixed infall velocity of the Local Group (LG) into the centre of LSC and because H_0 was fixed from external considerations the distance to centre of LSC became to be $R_{\rm Virgo} = 21\,\mathrm{Mpc}$. For further details of the TB-model adopted cf. Paper II. Additional discussion can be found in Paper I, Ekholm & Teerikorpi (1994) and Ekholm (1996).

The observed systemic velocity vs. distance $R_{\rm gal}$ diagrams are presented in Figs. 1-5. In the first four figures galaxies belonging to a $\Theta < 30^\circ$ cone are shown for different angular intervals: galaxies having $\Theta < 10^\circ$ are shown as black bullets, galaxies having $10^\circ \le \Theta < 20^\circ$ as grey bullets and galaxies having $20^\circ \le \Theta < 30^\circ$ as circles. The TB-curves are given for the mean angular distance, $\langle\Theta\rangle$, for each angular interval as thick black curve for $\langle\Theta\rangle = 4.5^\circ$, as thick grey curve for $\langle\Theta\rangle = 15.6^\circ$ and as thin black curve for $\langle\Theta\rangle = 25.8^\circ$. Comparison between the data and the mean predictions were made for different presumed distances to the centre of LSC: $R_{\rm Virgo} = 16\,\mathrm{Mpc}$ (Fig. 1), $R_{\rm Virgo} = 18\,\mathrm{Mpc}$ (Fig. 2), $R_{\rm Virgo} = 21\,\mathrm{Mpc}$ (Fig. 3) and $R_{\rm Virgo} = 24\,\mathrm{Mpc}$ (Fig. 4). We remind that our model is formulated in terms of the relative distance $d_{\rm gal} = R_{\rm gal}/R_{\rm Virgo}$. So the TB-curves show different behaviour depending on the normalization.

The thick black line in each figure corresponds to the Hubble law based on $H_0 = 75\,\mathrm{km\,s^{-1}\,Mpc^{-1}}$, $H_0 =$

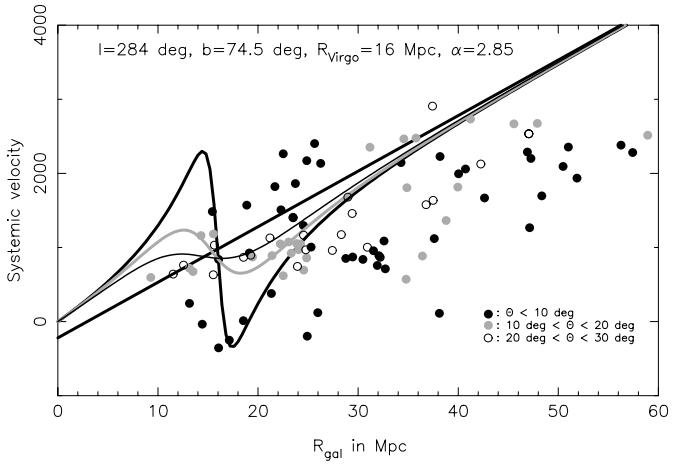

Fig. 1. The systemic velocity vs. distance for galaxies listed in Table 1 for the Model 1 and $R_{\rm Virgo} = 16$ Mpc. The data points are given with black bullets for $\Theta < 10^\circ$, with grey bullets for $10^\circ \leq \Theta < 20^\circ$ and with circles for $20^\circ \leq \Theta < 30^\circ$. The thick black curve is the theoretical TB-pattern for the average angular distance $\langle\Theta\rangle = 4.5^\circ$, the gray curve is for $\langle\Theta\rangle = 15.6^\circ$ and the thin black curve for $\langle\Theta\rangle = 25.8^\circ$. These values are the mean values of data in each angular interval. The straight line is the Hubble law for $H_0 = 75\,\mathrm{km\,s^{-1}\,Mpc^{-1}}$ based on the adopted distance and $V_{\rm Virgo}^{\rm cosm} = 1200\,\mathrm{km\,s^{-1}}$.

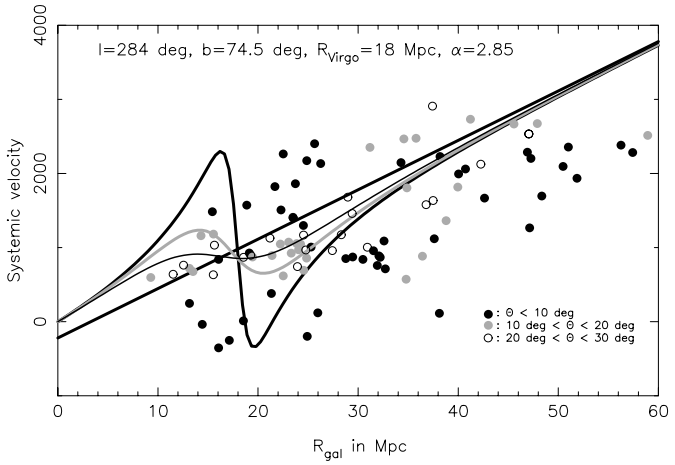

Fig. 2. As Fig. 1, but now the distance to Virgo used for normalization is $R_{\rm Virgo} = 18$ Mpc, which corresponds to $H_0 = 67\,\mathrm{km\,s^{-1}\,Mpc^{-1}}$.

$67\,\mathrm{km\,s^{-1}\,Mpc^{-1}}$, $H_0 = 57\,\mathrm{km\,s^{-1}\,Mpc^{-1}}$ and $H_0 = 50\,\mathrm{km\,s^{-1}\,Mpc^{-1}}$, respectively. The line is drawn through the centre of LSC in order to emphasize our basic assumption that the centre is at rest with respect to the cosmological background. This also allows one to appreciate the infall of the Local Group with an assumed velocity $V_{\rm LG}^{\rm in} = 220\,\mathrm{km\,s^{-1}}$.

Figs. 1 and 2 immediately reveal that the shorter distances are not acceptable because the background galaxies fall far below the expected curves. Correction for any residual Malmquist bias would make situation even worse. Neither is $R_{\rm Virgo} = 21$ Mpc, the distance found favourable in Paper II, totally satisfying. Although the clump of galaxies at $R_{\rm gal} \sim 32$ Mpc and

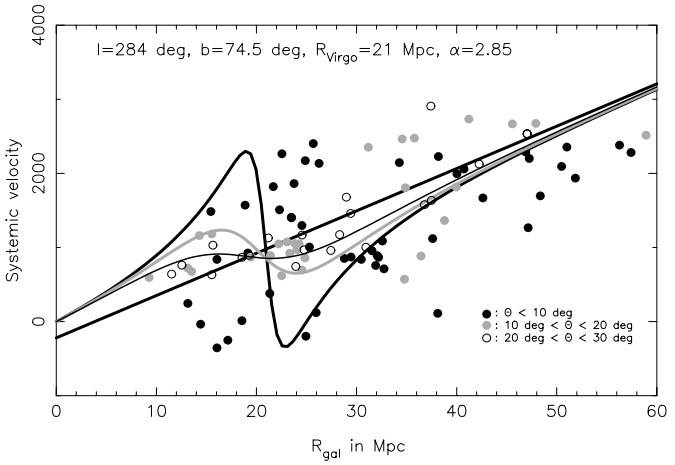

Fig. 3. As Fig. 1, but now the distance to Virgo used for normalization is $R_{\rm Virgo} = 21$ Mpc, which corresponds to $H_0 = 57\,\mathrm{km\,s^{-1}\,Mpc^{-1}}$.

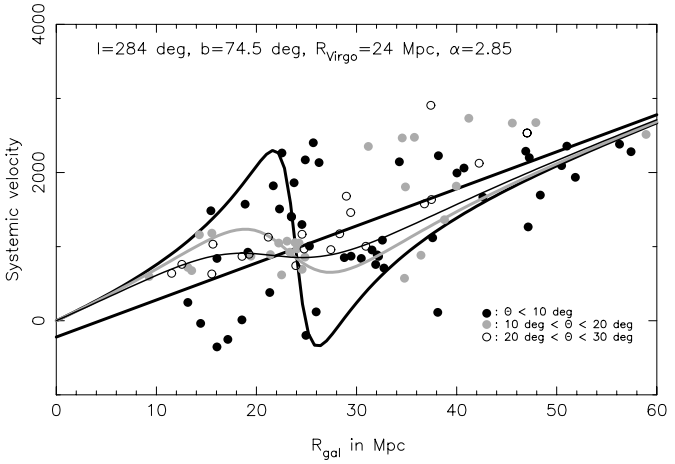

Fig. 4. As Fig. 1, but now the distance to Virgo used for normalization is $R_{\rm Virgo} = 24$ Mpc, which corresponds to $H_0 = 50\,\mathrm{km\,s^{-1}\,Mpc^{-1}}$.

$V_{\rm sys} \sim 800\,\mathrm{km\,s^{-1}}$ in Fig. 3 follow the prediction as some other galaxies, the maximum of the velocity amplitude is clearly behind the presumed centre.

This led us to test a longer distance to Virgo. The result is shown in Fig. 4. It is rather remarkable that such a distance gives better fit than the shorter ones. On the other hand $R_{\rm Virgo} = 24$ Mpc together with the adopted cosmological velocity bring about $H_0 = 50\,\mathrm{km\,s^{-1}\,Mpc^{-1}}$. Such a small value has for decades been advocated by Sandage and his collaborators and is within the error bars of our determinations (Theureau et al. 1997; Ekholm et al. 1999b) as well. It is encouraging that galaxies outside the 30° cone follow well the Hubble law for this H_0. Virgo has only a weak influence on them, and if the Malmquist bias is present these galaxies should predict *larger* value for H_0. The dashed line in Fig. 5 is the Hubble law for $H_0 = 60\,\mathrm{km\,s^{-1}\,Mpc^{-1}}$. It is clearly an upper limit thus giving us a lower limit for the distance to Virgo: $R_{\rm Virgo} \geq 20$ Mpc.

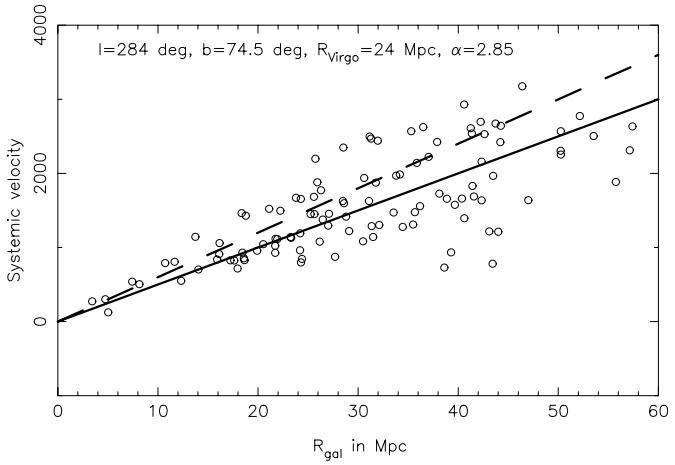

Fig. 5. The systemic velocity vs. distance for galaxies outside the $\Theta = 30^\circ$ cone but still having $V_{\rm obs} \leq 3 \times V_{\rm Virgo}^{\rm cosm} \cos\Theta$ and $R_{\rm gal} \leq 60\,{\rm Mpc}$. The solid line is the Hubble law predicted by $H_0 = 50\,{\rm km\,s^{-1}\,Mpc^{-1}}$ and the dashed line the Hubble law predicted by $H_0 = 60\,{\rm km\,s^{-1}\,Mpc^{-1}}$.

4. Have we found the true TB signature of Virgo?

So far we have studied the $V_{\rm sys}$ vs. $R_{\rm gal}$ diagram in a simple way by moving the curves for the TB-solution by choosing different normalizing distances to Virgo. The best agreement with the maximum observed amplitude and the curves was found at a rather large distance, namely $R_{\rm Virgo} = 24\,{\rm Mpc}$. Such a long distance leads one to ask whether we have actually found Virgo. We examine this question by comparing our sample given in Table 1 with the sample given by Federspiel et al. (1998) from which they found $R_{\rm Virgo} = 20.7\,{\rm Mpc}$. We found 33 galaxies in common when requiring $\Theta < 6^\circ$. We present these galaxies in Fig. 6. For an easy reference each galaxy is assigned a number given also as a superscript after the name in Table 1.

We give each galaxy a symbol following the classification of Federspiel et al. (1998). Following Binggeli et al. (1993) galaxies were divided into subgroup "big A" for galaxies close to M87 ('A') and into "B" for galaxies within $2\overset{\circ}{.}4$ of M49 ('B'). They also examined whether a galaxy is within the X-ray isophote $0.444\,{\rm counts\,s^{-1}\,arcmin^{-1}}$ based on ROSAT measurements of diffuse X-ray emission of hot gas in the Virgo cluster (Böhringer et al. 1994) ('A,X', 'B,X'). Galaxies belonging to subgroup A and within the X-ray contour are labelled in Fig. 6 as bullets and outside the contour with an open circle. Similarly, galaxies in subgroup B are labelled with a filled or open triangle. Federspiel et al. also listed galaxies within the X-ray contour but not classified as members of A or B. The galaxies are marked with a filled square. They also included in their Table 3 some galaxies which fall outside A and B and the X-ray contour (we label them with an open square).

We also give an error estimate for the TF-distance for each galaxy calculated from the 1σ error in the distance modulus:

$$\sigma_\mu = \sqrt{\sigma_B^2 + \sigma_{M_p}^2}. \qquad (3)$$

The error in the corrected total B-band magnitude is taken from Column (8) in our Table 1 and the intrinsic dispersion of the absolute magnitude M for each p, σ_{M_p} is estimated to be $0.3^{\rm mag}$.

The straight solid line is the Hubble law for $H_0 = 50\,{\rm km\,s^{-1}\,Mpc^{-1}}$ shifted downwards by $V_{\rm LG}^{\rm in} = 220\,{\rm km\,s^{-1}}$ in order to make the line go through the centre at $R_{\rm Virgo} = 24\,{\rm Mpc}$ which is presumed to be at rest with respect to the cosmological background. The TB-curves are given for $\Theta = 2^\circ$ (thick black curve), $\Theta = 3\overset{\circ}{.}5^\circ$ (thick grey curve) and $\Theta = 5^\circ$ (thin black curve), respectively.

To begin with, there are 22 galaxies (67%) which agree with the TB-solution within 1σ in σ_μ. Only four galaxies (1,3,19,26; 12%) [2] do not agree with the model within 2σ. Though we have not reached the traditional 95% confidence level, the agreement is, at the statistical level found, satisfying enough. Furthermore, we find in the range $R = 24 \pm 2\,{\rm Mpc}$ nine galaxies out of which seven were classified by Federspiel et al. (1998) as 'A,X' galaxies hence presumably lying in the very core of Virgo. The remaining two galaxies are 'A' galaxies. In the range $R = 16 \pm 2\,{\rm Mpc}$ we find only three 'A,X' galaxies and one 'A' galaxy. Federspiel et al. (1998) following Guhathakurta et al. (1988) listed five galaxies (17, 18, 19, 20 and 26 in Table 1) as HI-deficient. If these galaxies are removed one finds four 'A,X' and two 'A' galaxies in the range $R = 24 \pm 2\,{\rm Mpc}$, and one 'A,X' and one 'A' galaxy in the range $R = 16 \pm 2\,{\rm Mpc}$. The numbers are still clearly more favorable for a long distance to Virgo.

Four galaxies in this sample have also distances from the extragalactic PL-relation (Lanoix 1999; Lanoix et al. 1999a, 1999b, 1999c). These galaxies are NGC 4321 (13) with $R_{PL} = 15.00\,{\rm Mpc}$, NGC 4535 (23) with $R_{PL} = 15.07\,{\rm Mpc}$, NGC 4548 (24) with $R_{PL} = 15.35\,{\rm Mpc}$ and NGC 4639 (28) with $R_{PL} = 23.88\,{\rm Mpc}$. These positions are shown as diamonds in Fig. 6. The mean distance to Virgo using the 'A,X' galaxies 13, 21, 24, 27, 28, 29 and 32 (i.e. the HI-deficient galaxies excluded) with TF-distance moduli is $\langle\mu\rangle = 31.81$ or $\langle R_{\rm Virgo}\rangle = 22.98\,{\rm Mpc}$ and when using the PL-distance moduli available for the three galaxies (13, 24 and 28) $\langle\mu\rangle = 31.60$ or $\langle R_{\rm Virgo}\rangle = 20.93\,{\rm Mpc}$. The difference is not large, and in both cases these Virgo core galaxies predict a distance $R_{\rm Virgo} > 20\,{\rm Mpc}$. We find also some other interesting features in Fig. 6. There are three galaxies (15, 16 and 22) which Federspiel et al. (1998) classified as 'B,X' and two (11,12) classified as 'B'. Together they form a clearly distinguishable substructure. It is the region D of Paper I, there interpreted as a tight background concentration. The mean distance for 'B,X' galaxies is $\langle R\rangle = 30.61\,{\rm Mpc}$ corresponding to $\mu = 32.43$. This region is $0.53^{\rm mag}$ more distant than our presumed centre. We find this result satisfying because Federspiel et al. (1998) estimated that the subgroup 'B' (region D in Paper I) is, on average, about $0.46^{\rm mag}$ farther distance than subgroup 'A'. That

[2] Also NGC 4216 (7) should probably be counted to this group, because it differs by $\sim 2\sigma$ and clearly belongs to the same substructure as the other four disagreeing galaxies. In other words, 15% of the sample does not agree with the model within 2σ.

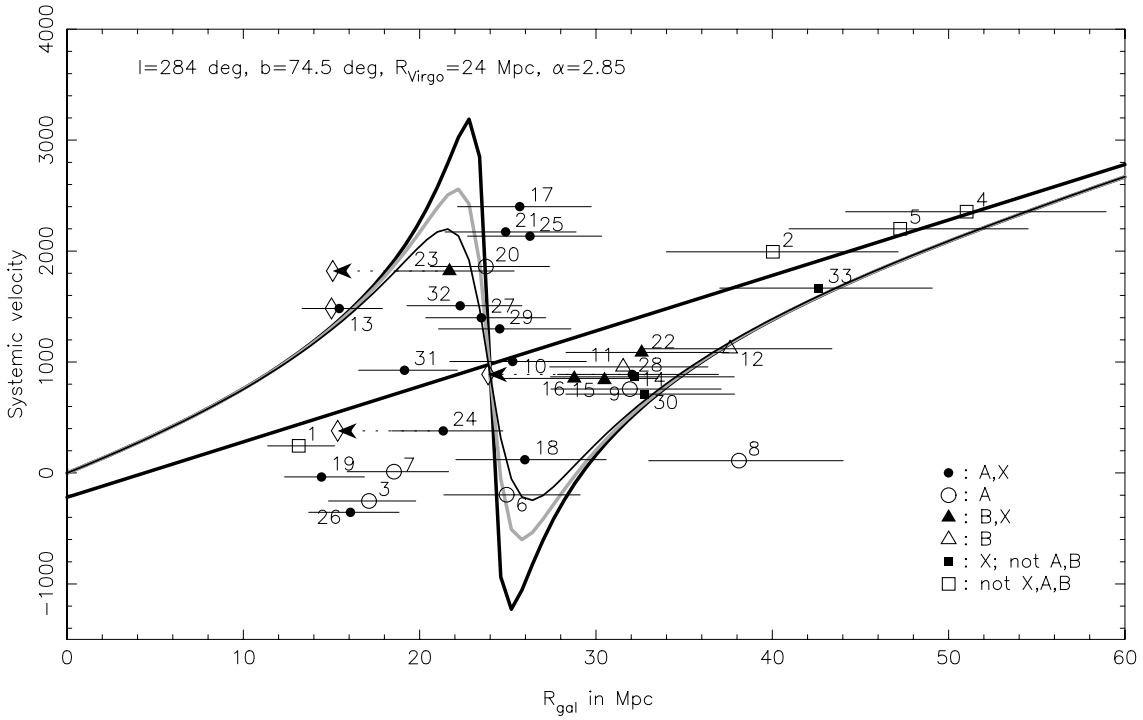

Fig. 6. The systemic velocity vs. distance diagram for the 33 galaxies common in Table 1 in this paper and Table 3 in Federspiel et al. (1998).

our sample brings about approximately the correct relative distance between these subgroups lends additional credence to the distance estimation made in the previous section.

The region B of Paper I described as an expanding component is also conspicuously present in Fig. 6 [3]. There is, however, no clear trace of the region C of Paper I (galaxies of high velocities but lying behind the centre; cf. Fig. 8 in Paper I) unless NGC 4568 (25) actually lies at the same distance as NGC 4567 ($R = 34.28$ Mpc). It should be remembered that NGC 4567/8 is classified as an interacting pair. There are, however, in Fig. 4 many galaxies at larger angular distances around NGC 4567. It is possible that they form the region C. In Paper I region C was divided into two subregions, C1 and C2. C1 was interpreted as the symmetrical counterpart to the region B (these galaxies behind Virgo are expanding away from it) and C2 was considered as a background contamination. Galaxies in region A (galaxies with high velocities lying in front of the centre) were proposed in Paper I to be presently falling into Virgo. As regards regions A and C1 it is now easy to understand that they are not separate regions but reflect the behaviour of the TB-curve: A is on the rising part and C1 on the declining part of the curve in front of the structure.

We conclude that from the expected distance-velocity pattern we have accumulated quite convincing evidence for a claim that the distance to the Virgo cluster is $R_{\rm Virgo} = 20-24$ Mpc or in terms of the distance modulus $\mu = 31.51-31.90$. $\Delta\mu = 0.39$ is within 1σ uncertainty of our TF-sample.

5. The velocity field as seen from the centre of LSC

In the first part of this paper we have approached the problem of the dynamical behaviour of LSC in a more or less qualitative manner. We now proceed to present the results in a physically more relevant manner. The main difficulty in the presentation used e.g. in Figs. 1- 4 is that the systemic velocity depends not only on the distance from LG but also on the angular distance from the centre. Basically, for each galaxy there is a unique "S-curve" depending on Θ.

Formally, the Θ-dependence is removed if the velocity-distance law is examined from the origin of the metric instead of from LG, as was done in Sect. 4.5 of Paper I. The velocity as seen from Virgo for a galaxy is solved from:

$$v(d_{\rm c}) = \pm \frac{V_{\rm obs}(d_{\rm gal}) - V^{\rm obs}_{\rm Virgo}\cos\Theta}{\sqrt{1-\sin^2\Theta/d_{\rm c}^2}}. \qquad (4)$$

The relative distance from the centre $d_{\rm c} = R_{\rm c}/R_{\rm Virgo}$, where $R_{\rm c}$ is the distance between the galaxy considered and the centre of Virgo, is solved from Eq. 14 of Paper II and the sign is $(-)$ for $d_{\rm gal} < \cos\Theta$ and $(+)$ otherwise.

There are, however, some difficulties involved. We are aware that the calculation of the virgocentric velocity is hampered by some sources of error. Suppose that the cosmological fluid has a perfect radial symmetry about the origin of the TB-metric. Also, the fluid elements do not interact with each other, i.e. each

[3] That such galaxies with negative velocity may be within a small angular distance from the Virgo cluster and still be well in the foreground was explained in Paper I as due to two things: 1) The expansion velocity must decrease away from the massive Virgo, and 2) because of projection effects, the largest negative velocities, belonging to galaxies at small distances from Virgo, are seen close to the Virgo direction.

element obeys *exactly* the equations of motion of the TB-model. It follows that the measured line-of-sight velocity is a genuine projection of the element's velocity with respect to the origin. It is presumed that the observer has made the adequate corrections for the motions induced by his immediate surroundings (e.g. Sun's motion with respect to the Galaxy, Galaxy's motion with respect to the LG).

Now, in practice, $V_{\rm obs}$ is bound to contain also other components than simply the TB-velocity. We may also have mass shells which have travelled through the origin and are presently expanding near it instead being falling in. Such a shell has experienced strong pressures (in fact, a singularity has formed to the origin) i.e. there is no causal connection to the rest of the TB-solution. Also, shells may have crossed. Again singularity has formed and the TB-solution fails (recall that TB-model describes a *pressure-free* cosmological fluid). Incorrect distance $R_{\rm gal}$ (and the scaling length $R_{\rm Virgo}$) will cause an error in $v(d_{\rm c})$ even when $V_{\rm obs}$ could be considered as a genuine projection of $v(d_{\rm c})_{\rm TB}$.

5.1. The two-component mass model

So far we have used a rather simple density model. From hereon we use the "two-component" model of Paper I. In this model one assumes that mass within $\Theta = 6^\circ$ at Virgo distance ($d_{\rm virial} = 0.105$) is proportional to the Virgo virial mass and that outside this region the mass is evaluated from the simple density law (Eq. 9 in Paper II):

$$M(d_{\rm c}) = M(d_{\rm c})_\alpha - M(d_{\rm virial})_\alpha + \beta M_{\rm virial}. \tag{5}$$

The important quantity is the parameter $A(R, T_0)$ (Eq. 6 in Paper II). Following Ekholm (1996) we now proceed to express it in terms of the relative distance "measured" from the origin of the metric $d \equiv d_{\rm c}$ and the deceleration parameter q_0. In terms of d it reads:

$$A(d, T_0) = \sqrt{\frac{GM(d)}{d^3 R_{\rm Virgo}^3}} \times T_0. \tag{6}$$

Because (cf. Eq. 9 in Paper II)

$$M(d)_\alpha = \frac{q_0 H_0^2}{G} d^3 R_{\rm Virgo}^3 [1 + k'\, d^{-\alpha}], \tag{7}$$

we find

$$A(d, T_0) = H_0 T_0 \sqrt{q_0}\,[1 + k' d^{-\alpha} - (d_{\rm virial}/d)^3 (1 + k' d_{\rm virial}^{-\alpha}) + (\beta G M_{\rm virial})/(d^3 R_{\rm Virgo}^3 H_0^2)]^{1/2}. \tag{8}$$

Now, using $M_{\rm virial} = 7.5 \times 10^{14} M_\odot R_{\rm Virgo}/16.8$ Mpc, $H_0 T_0 = C(q_0)$ (e.g. the function $C(q_0) = 2/3$ for $q_0 = 0.5$) and $H_0 R_{\rm Virgo} = V_{\rm Virgo,cosm}$, Eq. 8 takes its final form

$$A(d, q_0) = C(q_0)\sqrt{q_0}\,[1 + k' d^{-\alpha} - (d_{\rm virial}/d)^3 (1 + k' d_{\rm virial}^{-\alpha}) + (\beta \times {\rm cst})/(d^3 V_{\rm Virgo,cosm}^2)]^{1/2}, \tag{9}$$

where ${\rm cst} = 7.5 \times 10^{14} M_\odot G/16.8\,{\rm Mpc} = 1.92 \times 10^5\ {\rm km^2\,s^{-2}}$.

5.2. $v(d_{\rm c})$ vs. $d_{\rm c}$ diagram for $R_{\rm Virgo} = 24$ Mpc

We show the virgocentric diagram for $R_{\rm Virgo} = 24$ Mpc in the left panel of Fig. 7. The galaxies are now selected in the following manner. From the initial sample we take galaxies having $0.105 < d_{\rm c} \leq 1.0$ but make no restriction on Θ. In this way we get a symmetric sample around the centre. Because the angular dependence is no longer relevant, we show the data for different ranges of $\log V_{\rm max}$: black bullets are for $\log V_{\rm max} \geq 2.4$, grey bullets for $\log V_{\rm max} \in [2.3, 2.4[$, circles for $\log V_{\rm max} \in [2.2, 2.3[$ and triangles for $\log V_{\rm max} \in [2.1, 2.2[$. The straight line is Hubble law as seen from the centre and the curves (predicted velocity $v'(d_{\rm c})$ vs. $d_{\rm c}$) correspond to different solutions to the two-component model. We have assumed $\alpha = 2.5$ and solved the TB-equations with Eq. 9 for $\beta = 0.5$, 1.0, 1.5 and 2.0 yielding mass excesses $k' = 0.701$, 0.504, 0.307 and 0.109, respectively.

Because the gradient of the $v'(d_{\rm c})$-curve gets quite steep as $d_{\rm c} \to 0$, it is easier to study the difference between calculated and predicted velocities

$$\Delta v(d_{\rm c}) = v(d_{\rm c}) - v'(d_{\rm c}) \tag{10}$$

as a function of $d_{\rm c}$. This is shown in the right panel of Fig. 7. The model values $v'(d_{\rm c})$ were based on $\beta = 2.0$. In this panel we also show the mean Δv for each $\log V_{\rm max}$ range. For $\log V_{\rm max} \geq 2.4$ ($N = 9$, $\Delta v = 579\ {\rm km\,s^{-1}}$) it is given as a black thick line, for $\log V_{\rm max} \in [2.3, 2.4[$ ($N = 26$, $\Delta v = 646\ {\rm km\,s^{-1}}$) as a grey thick line, for $\log V_{\rm max} \in [2.2, 2.3[$ ($N = 76$, $\Delta v = 359\ {\rm km\,s^{-1}}$) as a dashed line, and for $\log V_{\rm max} \in [2.1, 2.2[$ ($N = 55$, $\Delta v = 385\ {\rm km\,s^{-1}}$) as a dotted line. We note that our sample is clearly divided into two subgroups by $\log V_{\rm max} = 2.3$. The slower rotators show a better fit to our chosen model. In general, galaxies in this sample have on average higher velocities than the model predicts, possibly due to some residual Malmquist bias (cf. also Figs. 5 – 6 of Paper I). It is, however, clear that the overall TB-pattern is seen in the left panel of Fig. 7 as a general decrease in $v(d)_{\rm c}$ when one approaches the centre.

5.3. Evidence from galaxies with PL-distances

How do the galaxies with PL-distances behave in this virgocentric representation? When selected in a similar fashion as above we find 23 galaxies shown in Fig. 8. We saw that $R_{\rm Virgo} = 24$ Mpc was a rather high value for them but now $R_{\rm Virgo} = 21$ Mpc together with $\alpha = 2.5$ and $\beta = 2.0$ brings about a remarkable accordance. This is particularly important in the light of the complications mentioned in the introduction to this section. It seems that at least when using high quality distances such as PL-distances those difficulties do not hamper the diagrams significantly. When this result is compared with the findings of Paper II, the distance estimate given there seems to be more and more acceptable.

There are four galaxies which show anomalous behaviour. NGC 2541 is a distant galaxy as seen from Virgo ($R_{\rm gal} = 11.59$ Mpc, $\Theta = 63.8^\circ$, $V_{\rm obs} = 645\ {\rm km\,s^{-1}}$) and is also close to the tangential point where small errors in distance cause large projection errors in velocity. We tested how much one

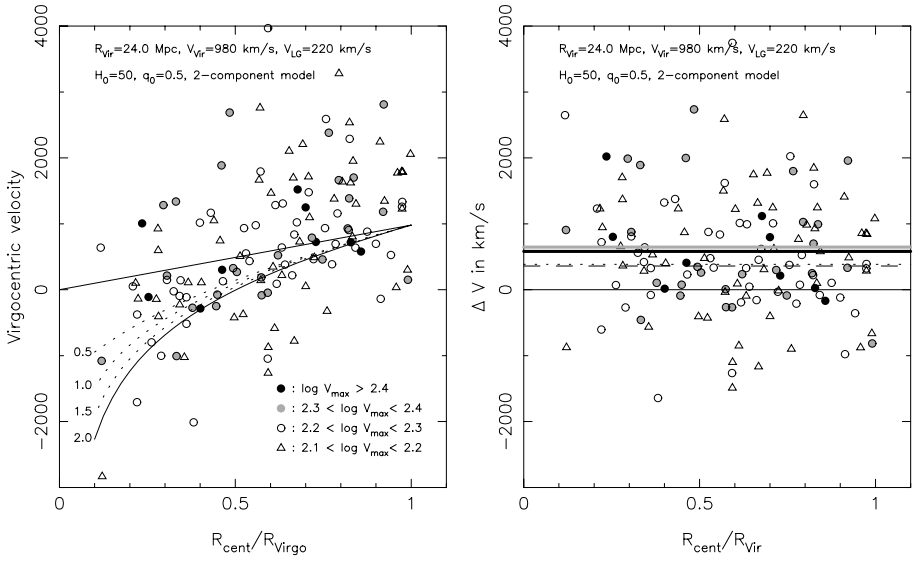

Fig. 7. Left panel: The virgocentric velocity as a function of TF-distance from the centre for $R_{\rm Virgo} = 24$ Mpc. The solid line is the Hubble law one would see from the centre and the curves are the TB-predictions for the two-component model (for details cf. text). Right panel: comparison between the calculated and predicted ($\beta = 2.0$, $\alpha = 2.5$) virgocentric velocities.

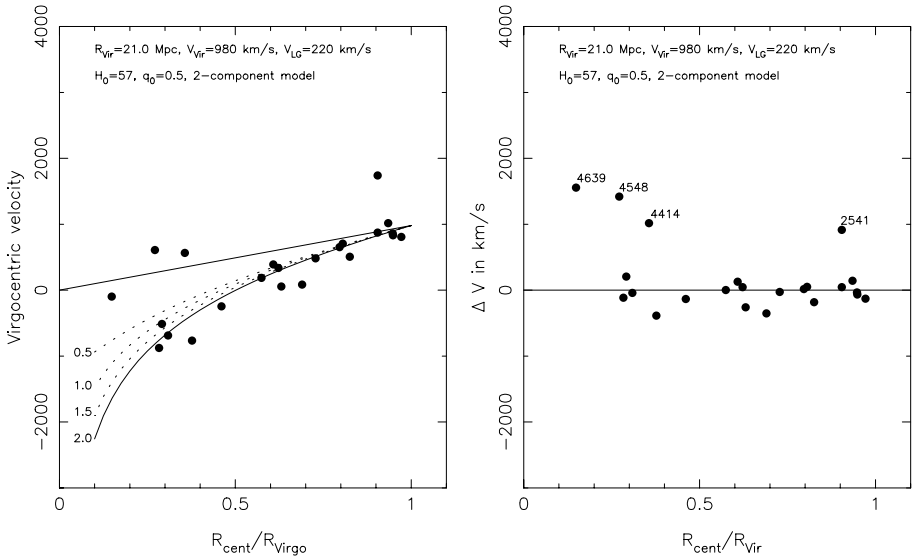

Fig. 8. Left panel: The virgocentric velocity vs. distance for the 23 galaxies with PL-distances. The relative distances are based on $R_{\rm Virgo} = 21$ Mpc. Right panel: comparison between calculated and predicted velocities for $\beta = 2.0$, $\alpha = 2.5$.

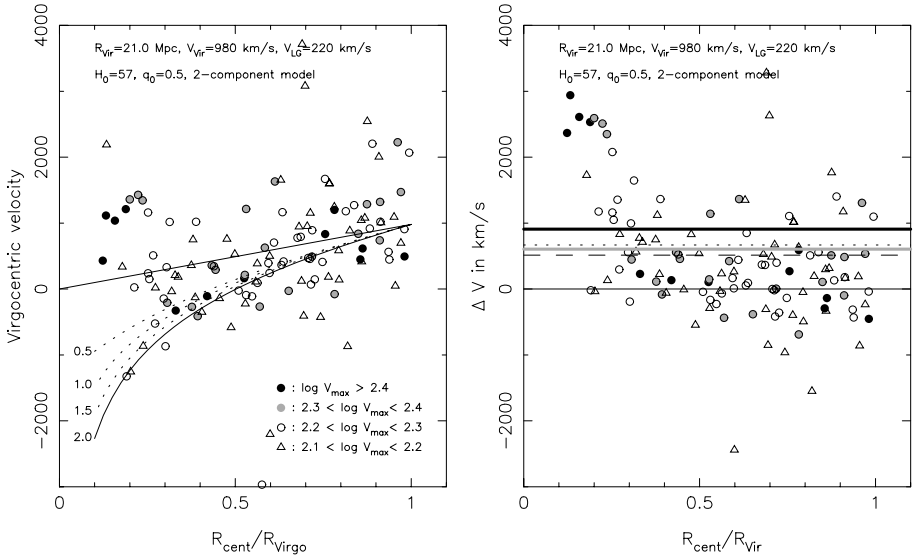

Fig. 9. As Fig. 7, but now the distance to Virgo is $R_{\rm Virgo} = 21$ Mpc.

needs to move this galaxy in order to find the correct predicted velocity. At $R_{\rm gal} = 13.93\,{\rm Mpc}$, $V_{\rm pred} = 645.1\,{\rm km\,s^{-1}}$ and $v(d_{\rm c}) = 884.7\,{\rm km\,s^{-1}}$ with $\Delta v = -0.5\,{\rm km\,s^{-1}}$. Note also that even a shift of $1\,{\rm Mpc}$ to $R_{\rm gal} = 12.59\,{\rm Mpc}$ will yield $\Delta v = 360.0\,{\rm km\,s^{-1}}$, which is quite acceptable. When NGC 4639 ($R_{\rm gal} = 23.88\,{\rm Mpc}$, $\Theta = 3.0°$, $V_{\rm obs} = 888\,{\rm km\,s^{-1}}$) is moved to $R_{\rm gal} = 21.0\,{\rm Mpc}$, one finds $V_{\rm pred} = 886.8\,{\rm km\,s^{-1}}$ and $v(d_{\rm c}) = -3419.5\,{\rm km\,s^{-1}}$ with $\Delta v = 45.6\,{\rm km\,s^{-1}}$. What is interesting in this shift is that in Paper II most of the galaxies tended to support $R_{\rm Virgo} = 21\,{\rm Mpc}$ except this galaxy and NGC 4548. Now NGC 4639 fits perfectly. Recently Gibson et al. (1999) reanalyzed some old HST measurements finding for NGC 4639: $\mu = 31.564$ or $R_{\rm gal} = 20.55\,{\rm Mpc}$. As regards the two other discordant galaxies (NGC 4414 and NGC 4548) the shift to remove the discrepancy would be too large to be reasonable. At this point we cannot explain their behaviour except by assuming that they are region B galaxies of Paper I (cf. below).

Also, when galaxies with TF-distances were selected according to this normalizing distance we find better concordance with the model than for $R_{\rm Virgo} = 24\,{\rm Mpc}$ (cf. Fig. 9). Note also that now only the fastest rotators differ from the rest of the sample: for $\log V_{\rm max} \geq 2.4$: $N = 12$, $\Delta v = 904\,{\rm km\,s^{-1}}$ (black thick line), for $\log V_{\rm max}[2.3, 2.4[$: $N = 23$, $\Delta v = 602\,{\rm km\,s^{-1}}$ (grey thick line), for $\log V_{\rm max} \in [2.2, 2.3[$: $N = 65$, $\Delta v = 512\,{\rm km\,s^{-1}}$ (dashed line) and for $\log V_{\rm max} \in [2.1, 2.2[$: $N = 49$, $\Delta v = 665\,{\rm km\,s^{-1}}$ (dotted line). At relatively large distances from the centre the points in the right panel of Fig. 9 follow on average well a horizontal trend. As one approaches the centre one sees how the velocity difference Δv gets larger and larger. This systematic increase explains why the mean values are so high. Note that also the Cepheid galaxies NGC 4414 and NGC 4548 (and NGC 4639 if one accepts the larger distance) show a similar increasing tendency towards the centre.

Because the inward growth of Δv appears for both distance indicators one suspects that this behaviour is a real physical phenomenon (we cannot explain it in terms of a large scatter in the TF-relation). Neither can we explain it by a bad choice of model parameters: the effect is much stronger than the variations between different models. A natural explanation is an expanding component (referred to above as region B): galaxies with very high Δv are on mass shells which have fallen through the origin in past and have re-emerged as a "second generation" of TB-shells. The very quick decay of the positive velocity residuals supports this picture. The mass of the Virgo cluster is expected to slow down these galaxies quite fast (Sect. 6 in Paper I), so the effect appears at small $d_{\rm c}$.

6. Discussion

We found using the two-component mass model (Eq. 5) and the high quality PL-distances (Fig. 8) an acceptable fit with parameters $\alpha = 2.5$ and $\beta \approx 2.0$. Our larger TF-sample did not disagree with this model though the scatter for these galaxies is rather large. β gives the Virgo cluster mass estimate in terms of the virial mass given by Tully & Shaya (1984). With a distance $R_{\rm Virgo} = 21\,{\rm Mpc}$ it is $M_{\rm TS} = 9.375 \times 10^{14} M_\odot$. By allowing some tolerance ($\beta = 1.5$ – 2.0) we get an estimate:

$$M_{\rm Virgo} = (1.4 - 1.875) \times 10^{15} M_\odot \tag{11}$$

6.1. The Virgo cluster mass, q_0, and behaviour of M/L

We have confirmed the large value of the mass-luminosity ratio for the Virgo cluster (Tully & Shaya 1984; Paper I):

$$(M/L)_{\rm Virgo} \approx 440\beta \times (16.8\,{\rm Mpc}/R_{\rm Virgo}). \tag{12}$$

With $\beta = 1$ – 2 and $R_{\rm Virgo} = 21\,{\rm Mpc}$, $(M/L)_{\rm Virgo}$ ranges from 350 to 700. Note that some calculations of Paper I for different q_0 (e.g. Table 2), which were based on $H_0 = 70\,{\rm km\,s^{-1}\,Mpc^{-1}}$ and $R_{\rm Virgo} = 16.5\,{\rm Mpc}$, remain valid when $H_0 = 55\,{\rm km\,s^{-1}\,Mpc^{-1}}$ and $R_{\rm Virgo} = (70/55) \times 16.5\,{\rm Mpc} = 21\,{\rm Mpc}$. For example, Fig. 7 of Paper I shows that if $(M/L)_{\rm Virgo}$ applies everywhere, rather high values of q_0 ($> 0.1 - 0.2$) are favoured. A very small q_0, say 0.01, would require that M/L outside of Virgo is several times smaller than in Virgo, i.e. the density of dark matter drops much more quickly than the density of luminous matter.

This happens also – though less rapidly – with $q_0 = 0.5$ used in this paper. This is seen from

$$\frac{(M/L)_{\rm sur}}{(M/L)_{\rm Virgo}} = \frac{M_{\rm sur}}{M_{\rm Virgo}} \times \frac{L_{\rm Virgo}}{L_{\rm sur}}. \tag{13}$$

The surroundings is defined as $d_{\rm c} \in]0.105, 1[$. The luminosity ratio is $L_{\rm Virgo}/L_{\rm sur} \approx 1/4$ (Tully 1982). The mass ratio is calculated using the two-component mass model (Eq. 5) with the help of Eq. 18 of paper II. For $M_{\rm Virgo} = 2$ the parameters needed are $k' = 0.109$, $\alpha = 2.5$, $q_0 = 0.5$ and $h_0 = 0.57$, which yield $M(d_{\rm c} = 1)_\alpha = 4.155$ and $M(d_{\rm c} = 0.105)_\alpha = 0.137$. We find $M_{\rm sur} = M(d_{\rm c} = 1)_\alpha - M(d_{\rm c} = 0.105)_\alpha = 4.018 \approx 4$. Both masses are given in units of the Virgo virial mass. The mass-luminosity ratio becomes $(M/L)_{\rm sur}/(M/L)_{\rm Virgo} \approx 0.5$. When $M_{\rm Virgo} = 1$ $(M/L)_{\rm sur}/(M/L)_{\rm Virgo} \approx 1.25$ and when $M_{\rm Virgo} = 1.5$ $(M/L)_{\rm sur}/(M/L)_{\rm Virgo} \approx 0.75$.[4] This means that with a Virgo mass slightly larger than the virial mass there is a case where the mass-luminosity ratio is constant in and outside Virgo.

How would luminous matter distribute itself? Consider the following simple exercise. Suppose the luminous matter follows a power law $\rho_{\rm lum}(r) \propto r^{-\alpha_{\rm lum}}$ and that the mass ratio is:

$$\frac{\int_{0.105}^{1} r^{2-\alpha} dr}{\int_{0}^{0.105} r^{2-\alpha} dr} = \frac{L_{\rm sur}}{L_{\rm Virgo}}. \tag{14}$$

With the luminosity ratio given above one derives for the galaxies $\alpha_{\rm lum} \approx 2.3$, indeed smaller than our preferred value of 2.5. Is such a steep value at all reasonable in the light of theoretical work on structure formation?

[4] The total mass within $d_{\rm c} = 1$ is 6.018 for $\beta = 2$, 6.019 for $\beta = 1$ and 6.020 for $\beta = 1.5$. The Model 1 of Paper II ($k' = 0.606$ and $\alpha = 2.85$) gives 6.017 as the total mass. Thus our computational scheme works correctly because the total mass should not depend on how we distribute the matter within our mass shell.

6.2. Comparison with the universal density profile

Tittley & Couchman (1999) discussed recently the hierarchical clustering, the universal density profile, and the mass-temperature scaling law of galaxy clusters. Using simulated clusters they studied the dark matter density profile in a Einstein-deSitter universe with $\Omega_{DM} = 0.9$, $\Omega_{\rm gas} = 0.1$ and $\Lambda = 0$. They assumed $H_0 = 65\,{\rm km\,s^{-1}\,Mpc^{-1}}$. Different profiles fitted their simulated data equally well. It is their discontinuous form in the first derivative which interests us:

$$\frac{\rho(r)}{\rho_c} = \begin{cases} \delta_{\gamma'} r^{-\gamma'}, & r < r_s \\ \delta_{\gamma} r^{-\gamma}, & r > r_s \end{cases} \tag{15}$$

They connect the overdensities as

$$\delta_\gamma = \frac{r_s^\gamma}{r_s^{\gamma'}} \delta_{\gamma'}. \tag{16}$$

Because the characteristic length $r_s < R_{200}$, where R_{200} is the radius where the density contrast equals 200, the near field governed by γ' is not important to us. With $\alpha = 2.5$ and $\beta = 2.0$ in our model the mass excess $k' = 0.109$. This translates into $k = (3-\alpha)\times k' R_{\rm Virgo}^\alpha/3 = 36.71$ in the density law of Paper II: $\delta(r) = \rho(r)/\rho_0 = 1 + kr^{-\alpha}$. ρ_0 is the background density equal to the critical density ρ_c when $q_0 = 0.5$. At the defined boundary of the Virgo cluster ($d = 0.105$ or $r = 2.205\,{\rm Mpc}$) we have a density excess $\delta = 5$. For $\beta = 1.5$, $k = 103.4$ and $\delta = 14.32$, and for $\beta = 1.0$, $k = 168.4$ and $\delta = 23.33$. Also, because $1 + kr^{-\alpha} \to kr^{-\alpha}$ as $r \to r_s$ comparison between our α and the γ of Tittley & Couchman is acceptable. For hierarchical clustering they find $\gamma = 2.7$ and for the non-hierarchical case $\gamma = 2.4$. The density profile fitting dynamical behaviour of the galaxies with PL-distances is within these limits. Our mass estimate tends to be closer to the maximum values Tittley & Couchman give in their Table 3.

7. Summary and conclusions

In this third paper of our series we have extended the discussion of Ekholm et al. (1999a; Paper II) to the background of Virgo cluster by selecting galaxies with as good distances as possible from the direct B-band magnitude Tully-Fisher (TF) relation. In the following list we summarize our main results:

1. Although having a rather large scatter the TF-galaxies reveal the expected Tolman-Bondi (TB) pattern well. We compared our data with TB-solutions for different distances to the Virgo cluster. It turned out that when $R_{\rm Virgo} < 20\,{\rm Mpc}$ the background galaxies fell clearly below the predicted curves. Hence the data does not support such distance scale (cf. Figs. 1 and 2).
2. When we examined the Hubble diagram for galaxies outside the Virgo $\Theta = 30^\circ$ cone (Fig. 5) we noticed that $H_0 = 60\,{\rm km\,s^{-1}\,Mpc^{-1}}$ is a clear upper limit for these galaxies. Together with our preferred cosmological velocity of Virgo ($1200\,{\rm km\,s^{-1}}$) we concluded that $R_{\rm Virgo} = 20\,{\rm Mpc}$ is a lower limit.
3. In both cases any residual Malmquist bias would move the sample galaxies further away and thus make the short distances even less believable.
4. We compared our sample galaxies with $\Theta < 6^\circ$ with the Table 3 of Federspiel et al. (1998) and found 33 galaxies in common. We established a plausible case for $R_{\rm Virgo} = 24\,{\rm Mpc}$ corresponding to $H_0 = 50\,{\rm km\,s^{-1}\,Mpc^{-1}}$ (cf. Fig. 6). The difference between $R_{\rm Virgo} = 20\,{\rm Mpc}$ and $R_{\rm Virgo} = 24\,{\rm Mpc}$ is – in terms of the distance moduli – only $\Delta\mu = 0.39$, which is within the 1σ scatter of the TF-relation. Due to this scatter it is not possible to resolve the distance to Virgo with higher accuracy. Hence we claim that $R_{\rm Virgo} = 20 - 24\,{\rm Mpc}$.
5. Some of the kinematical features identified in Paper I were revealed also here, in particular the concentration of galaxies in front with very low velocities (interpreted as an expanding component; region B in Paper I) and the tight background concentration (region D in Paper I). The symmetric counterpart of region B (region C1) may actually be part of the primary TB-pattern.
6. The need for a better distance indicator (e.g. the I-band TF-relation) is imminent. As seen e.g. from Fig. 9, the scatter in the B-band TF-relation is disturbingly large. It is also necessary to re-examine the calibration of the TF-relation with the new, and better, PL-distances. It seems that the PL-distances and the TF-distances from Theureau et al. (1997) are not completely consistent. The former tend to be somewhat smaller. This is also seen from Figs. 6 and 8. TF-distances support $R_{\rm Virgo} = 24\,{\rm Mpc}$ and PL-distances $R_{\rm Virgo} = 21\,{\rm Mpc}$. It is, however, worth reminding that our dynamical conclusions are insensitive to the actual distance scale.
7. When we examined the Hubble diagram as it would be seen from the origin of the TB-metric, galaxies with distances from the extragalactic PL-relation fitted best to a solution with $R_{\rm Virgo} = 21\,{\rm Mpc}$ in concordance with Paper II and with Federspiel et al. (1998). We are, however, not yet confident enough to assign any error bars to this value.
8. For $R_{\rm Virgo} = 21\,{\rm Mpc}$ the region D follows well the TB-pattern (cf. Fig. 3) lending some additional credence to this distance. We quite clearly identified this background feature as the subgroup "B" of Federspiel et al. (1998).
9. These high quality galaxies also clearly follow the expected velocity-distance behaviour in the virgocentric frame with much smaller scatter than for galaxies in Paper I or for the TF-galaxies used in this paper. The zero-velocity surface was detected at $d_{\rm c} \approx 0.5$.
10. As in Teerikorpi et al. (1992; Paper I), the amplitude of the TB-pattern requires that the Virgo cluster mass must be at least its standard virial mass (Tully & Shaya 1984) or more. Our best estimate is $M_{\rm Virgo} = (1.5 - 2) \times M_{\rm virial}$, where $M_{\rm virial} = 9.375 \times 10^{14} M_\odot$ for $R_{\rm Virgo} = 21\,{\rm Mpc}$.
11. Our results indicate that the density distribution of luminous matter is shallower than that of the total gravitating matter. The preferred exponent in the density power law, $\alpha \approx 2.5$, agrees with the theoretical work on the universal density

profile of dark matter clustering (Tittley & Couchman 1999) in the Einstein-deSitter universe.

Acknowledgements. This work has been partly supported by the Academy of Finland (project 45087: "Galaxy Streams and Structures in the nearby Universe" and project "Cosmology in the Local Galaxy Universe"). We have made use of the Lyon-Meudon Extragalactic Database LEDA and the Extragalactic Cepheid Database. We would like to thank the referee for useful comments.

References

Binggeli B., Popescu C.C., Tammann G.A., 1993, A&AS 98, 275
Böhringer H., Briel U.G., Schwartz R.A., et al., 1994, Nat 368, 828
Bondi H., 1947, MNRAS 107, 410
Ekholm T., 1996, A&A 308, 7
Ekholm T., Teerikorpi P., 1994, A&A 284, 369
Ekholm T., Lanoix P., Teerikorpi P., et al., 1999a, A&A 351, 827 (Paper II)
Ekholm T., Teerikorpi P., Theureau G., et al., 1999b, A&A 347, 99
Federspiel M., Tammann G.A., Sandage A., 1998, ApJ 495, 115
Gamow G., 1946, Nat 379, 549
Gibson B.K., Stetson P.B., Freedman W.L., et al., 1999, ApJ, in press (astro-ph/9908149)
Gouguenheim L., 1969, A&A 3, 281
Guhathakurta P., van Gorkum J.H., Kotanyi C.G., Balkowski C., 1988, AJ 96, 851
Hoffman G.L., Olson D.W., Salpeter E.E., 1980, ApJ 242, 861
Humason M.L., Mayall N.U., Sandage A., 1956, AJ 61, 97
Lanoix P., 1999, Ph.D. Thesis, University of Lyon 1
Lanoix P., Paturel G., Garnier R., 1999a, MNRAS 308, 969
Lanoix P., Garnier R., Paturel G., et al., 1999b, Astron. Nachr. 320, 21
Lanoix P., Paturel G., Garnier R., 1999c, ApJ 516, 188
Ogorodnikov K.F., 1952, Problems of Cosmogony 1, 150
Olson D.W., Silk J., 1979, ApJ 233, 395
Peebles J., 1976, ApJ 205, 318
Rubin V.C., 1951, AJ 56, 47
Rubin V.C., 1988, In: Corwin H.C., Bottinelli L. (eds.) World of Galaxies. Springer, New York, p. 431
Silk J., 1974, ApJ 193, 525
Teerikorpi P., 1997, ARA&A 35, 101
Teerikorpi P., Bottinelli L., Gouguenheim L., Paturel G., 1992, A&A 260, 17 (Paper I)
Theureau G., Hanski M., Ekholm T., et al., 1997, A&A 322, 730
Tittley E.R., Couchman H.M.P., 1999, astro-ph/9911365
Tolman R.C., 1934, Proc. Nat. Acad. Sci (Wash.) 20, 169
Tully R.B., Fisher J.R., 1977, A&A 54, 661
Tully R.B., 1982, ApJ 257, 389
Tully R.B., Shaya E.J., 1984, ApJ 281, 31
Vaucouleurs G. de, 1953, AJ 58, 30
Vaucouleurs G. de, 1958, AJ 63, 253
Vaucouleurs G. de, Vaucouleurs A. de, Corwin H.G., 1976, Second Reference Catalogue of Bright Galaxies. University of Texas Press, Austin (RC2)
Vaucouleurs G. de, Vaucouleurs A. de, Corwin H.G., et al., 1991, Third Reference Catalogue of Bright Galaxies. Springer-Verlag (RC3)
Yahil A., Tammann G.A., Sandage A., 1977, ApJ 217, 903